Article

Metal-Enhanced Ratiometric Fluorescence/Naked Eye Bimodal Biosensor for Lead Ions Analysis with Bifunctional Nanocomposite Probes

Linlin Liang, Feifei Lan, Shenguang Ge, Jinghua Yu, Na Ren, and Mei Yan

Anal. Chem., **Just Accepted Manuscript** • DOI: 10.1021/acs.analchem.6b04978 • Publication Date (Web): 24 Feb 2017

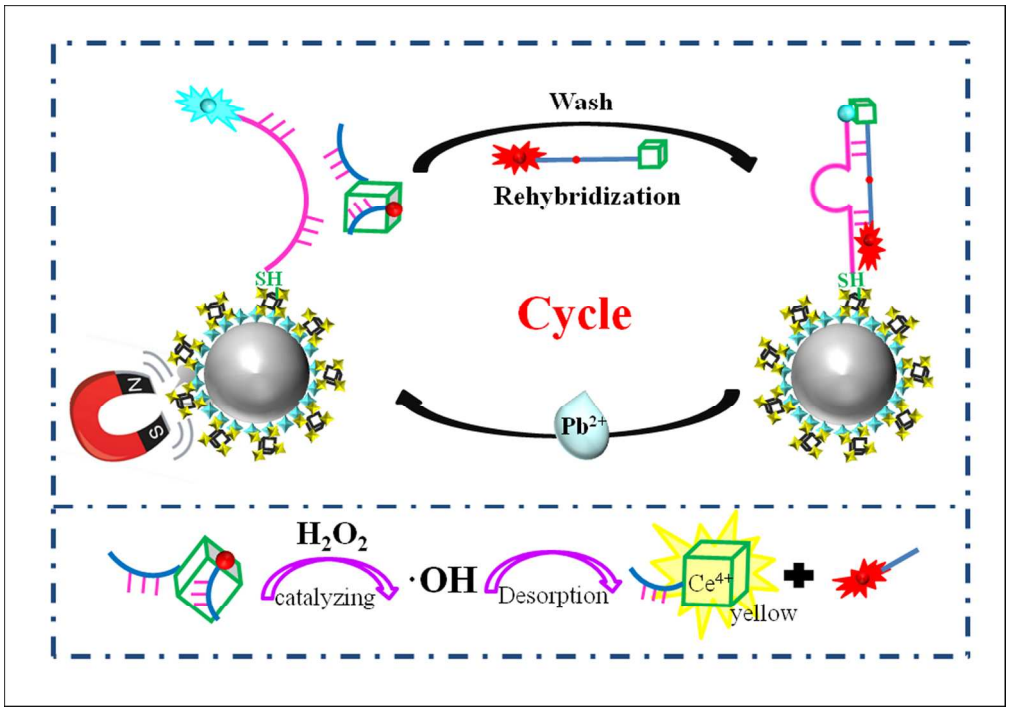

Graphical Abstract

152x106mm (300 x 300 DPI)

Metal-Enhanced Ratiometric Fluorescence/Naked Eye Bimodal Biosensor for Lead Ions Analysis with Bifunctional Nanocomposite Probes

Linlin Liang[a], Feifei Lan[a], Shenguang Ge[a,b*], Jinghua Yu[a], Na Ren[c], Mei Yan[a]

[a]School of Chemistry and Chemical Engineering, University of Jinan, Jinan 250022, P. R. China.

[b]Shandong Provincial Key Laboratory of Preparation and Measurement of Building Materials, University of Jinan, Jinan 250022, P.R. China.

[c]School of Biological Science and Technology, University of Jinan, Jinan 250022, P.R. China.

Abstract

A novel metal-enhanced ratiometric fluorescence/naked eye bimodal biosensor based on $ZnFe_2O_4$@Au-Ag bifunctional nanocomposite and DNA/CeO_2 complex for Pb^{2+} has been successfully developed. The nanocomposite probe was composed of a magnetic $ZnFe_2O_4$ core and a Au-Ag hollow nanocube shell. Upon bioconjugation, bifunctional magnetic nanocomposites could not only make the probe possess excellent recyclability, but also provide an enrichment of "hot spots" for surface enhanced fluorescence detection of Pb^{2+} by metal-enhanced fluorescence effect. Typically, the bifunctional nanocomposites conjugate with double-stranded DNA (included Pb^{2+}-specific DNAzyme strand and corresponding substrate strand) to form Pb^{2+} biosensor. Nanoceria as a fluorescence quencher strongly adsorbed DNA. Therefore, the formation of double-stranded DNA bringed the labeled N,S-CDs and CeO_2 into

close proximity, which significantly quenched the fluorescence of N,S-CDs. The presence of Pb^{2+} led to the breakage of the DNAzyme strand, resulting in the fluorescence signal of Cy3 decreased, while the fluorescence intensity of N,S-CDs aggrandized. Firstly, preliminary test of Pb^{2+} was performed by naked eye. The disengaged DNA/CeO_2 complex could result in color change after adding H_2O_2 because of autocatalysis of CeO_2, resulting in real-time visual detection of Pb^{2+}. If further accurate determination was required, by measuring the fluorescence intensity ratio of this two fluorescence indicators at 562 and 424 nm (I_{562}/I_{424}). A good linear correlation exists between the lg(I_{562}/I_{424}) and the logarithm of Pb^{2+} concentrations ranging from 10^{-12}-3×10^{-6} M. Remarkably, the detection limit of this ratiometric biosensor was 3×10^{-13} M, which ascribed to its superior fluorescence enhancement. Interestingly, the developed bifunctional nanocomposite probe manifests good recyclability and selectivity. More importantly, the biosensor provided potential application of on-site and real-time unknown Pb^{2+} ions in real systems.

Keywords: Ratiometric; $ZnFe_2O_4$@Au-Ag; DNA/CeO_2 complex; Metal-enhanced fluorescence; Visualization

1. Introduction

Signal amplification is considered to be a key point for sake of obtaining ultrahigh sensitive biosensors. Metal nanomaterials (such as Au and Ag) had metal-enhanced fluorescence (MEF) on nearby fluorophores, and the fluorescence emission could be enhanced by the MEF effect.[1,2] The MEF effect was highly correlated with type of metal nanoparticles[3] as well as distance between metal nanoparticles and fluorophores.[4] Compared with monometallic nanoparticles, bimetallic nanoparticles have received intensive study because of their remarkable properties, such as durability, biocompatibility and stability. In view of this, we prepared Ag-Au hollow nanocubes by means of galvanic replacement-free deposition of Au on Ag nanocubes with enhanced chemical stability and fluorescence enhancement activity.[5] In addition, in order to make the probe reutilize, magnetic nanoparticles were introduced. $ZnFe_2O_4$ reported by Su et al.,[6] one of the spinel ferrite compounds, was more stable with exposure to air and could be separated by means of a magnet. So, different biosensors based on magnetic nanoparticles were reported.[7,8] Up to now, bifunctional magnetic nanocomposites have attracted extensive attention because of the requirement of ultrasensitive biological assays and the trend of miniaturized analysis. Bifunctional magnetic nanocomposites could not only make the probe accessible for cyclic utilization, but also enhance fluorescence intensity by MEF effect, leading to lower and lower detection limits. Hence, bifunctional magnetic nanocomposites based biosensor opens the door for a series of basic research and provides new tools for detecting trace amounts of various analytes in environmental, industrial and clinical applications.

Nanoceria had attracted considerable interest because of its regeneration or autocatalysis.[9] When nanoceria was mixed with H_2O_2, resulting in a color change from colorless to orange in a concentration-dependent manner. So, the detection of H_2O_2 was achieved by the change of color.[10] In addition, nanoceria had been reported to strongly adsorb DNA and nucleotides based on electrostatic interactions.[11,12] The adjustable length and sequence of DNA also accelerates systematic research. Interestingly, nanoceria was a strong and general fluorescence quencher. These discoveries provide further potential in biosensor development and nanotechnology. However, the mechanism of quenching should not be resonance energy transfer. There might be electron transfer between nanoceria and fluorophores, which is a high band gap semiconductor.

Lead(II) (Pb^{2+}) ions, known as one of the nondegradable environmental pollutant, which have triggered a serious threat to human health such as irreversible brain damage and mental retardation.[13-15] Considering the potential biological accumulation and toxicity of lead to environment, therefore, ultrasensitive, reliable and recyclable detection of Pb^{2+} is highly desirable for water quality protection and disease prevention. In recent decades, newly several Pb^{2+} sensors have been developed.[16-25] Most of them are depended mainly on a "8-17" DNAzyme, which has the RNA nuclease activity to cleave the ribonucleotide, generating the change of detection signals. The DNAzyme has been used to realize sensitive detection of Pb^{2+} via different readout methods, such as electrochemical signals,[16,17] colorimetry[18,19] and fluorescence.[20-22] Because each method has its specific advantages as well as limitations, Synergistic combination of

two or more methods reach more reliable diagnostic results. For example, naked eye is the most commonly method on account of their simplicity, naked eye, simple instrumentation and low-cost, but relatively low sensitivity. In particular, the fluorescence methods have been paid extensive close attention due to their high sensitivity and the ability to provide in situ and real-time information. The naked eye method could be used for rapid screening and semi-quantitative analysis. If necessary, fluorescence detection was implemented accurate quantitative. Nevertheless, as the change in fluorescence intensity is the only test signal, factors such as environmental changes, the probe concentration and instrumental efficiency can interfere with the signal output.[26] Results may occur false positive or negative errors during the detection of trace level analytes. Ratiometric biosensors could effectively normalize the variation and make the detection more convincing.[27,28] Thus, a metal-enhanced ratiometric fluorescence/naked eye bimodal strategies have been developed.

Illuminated by these previous studies, in the present manuscript, a novel sensitive and selective ratiometric biosensor for Pb^{2+} was first designed by integrating the specific recognition of DNAzyme toward targets with $ZnFe_2O_4$@Au-Ag bifunctional nanocomposite and DNA/CeO_2 complex. The introduction of $ZnFe_2O_4$@Au-Ag bifunctional nanocomposite not only made this biosensor regenerate by supplementation of Cy3-17DS-CeO_2 because of its magnetism, but also enhanced fluorescence intensity by MEF effect, leading to a highly sensitive biosensor. CeO_2 is excellent fluorescence quencher, resulting in the fluorescence of N,S-CDs quenched with double-stranded DNA (dsDNA), while the fluorescence of Cy3 increased by MEF

effect. Besides, it also adsorbs DNA, the formation of DNA/CeO_2 complex, leading to the fluorescence of Cy3 quenched and N,S-CDs increased. This moment, N,S-CDs was close to the Ag-Au hollow nanocubes to enhance its fluorescence. In addition, it could be used for visually determined by the naked eye. Compared with the conventional Pb^{2+} biosensor, this approach provided acceptable reproducibility, high sensitivity, good stability, visual, recyclable and ratiometric in Pb^{2+} detection. More importantly, the novel biosensor could be used for highly accurate and reliable determination of unknown Pb^{2+} ions in environment monitoring with satisfying results.

2. Materials and methods

2.1. Materials and reagents

Poly(vinylpyrrolidone) (PVP-55 with MW≈55000) was purchased from Alfa Aesar. Silver trifluoroacetate (CF_3COOAg, ≥99.99%), iron trichloride hexahydrate ($FeCl_3·6H_2O$), sodium acetate anhydrous, sodium hydrosulfide hydrate ($NaHS·xH_2O$), hydrochloric acid (HCl, 37% in water) poly(diallyldimethylammonium chloride) (PDDA), cerium nitrate hexahydrate ($Ce(NO_3)_3·6H_2O$), tetrachloroauric acid ($HAuCl_4$) were all purchased from Sigma-Aldrich Chemical Co. (USA). Sodium acetate (NaAc), $FeCl_3·6H_2O$, ethylene glycol (EG), citric acid (99.9%), and L-cysteine (97.0%) were purchased from Aladdin (Shanghai, China). Zinc chloride ($ZnCl_2$) were obtained from Chemical Reagent Co. (Tianjin, China). All chemicals and solvents were analytical reagent grade or above. Ultrapure water obtained from a Millipore water purification system (resistivity ≥ 18.2 MΩ, MilliQ, Millipore) was used in all experiments.

The DNA in this study was synthesized and purified by Sangon Biotech Co., Ltd. (Jinan,

China) and its sequences was presented as follows:

Catalytic strand (DNA_1): 5'-HS-TTT TTT TTT TTT TTT TTT CAT CTC TTC TCC GAG CCG GTC GAA ATA GTG AGT-NH_3-3'

Pb^{2+} specific substrate (17DS): 5'-HOOC-ACT CAC TAT Ar GGA AGA GAT

2.2. Synthesis of the Au-Ag Hollow Nanocube

Preparation of Ag Nanocubes: The Ag nanocubes were obtained using a previously reported polyol method.[29] Typically, 20 mL of EG was added into a 100 mL round bottom flask and preheated at 150 ºC. Other reagents all dissolved in EG. Then, 0.24 mL of NaHS (3 mM) was first introduced. After 2 min, 2 mL of HCl (3 mM) was injected into above solution, followed by rapid addition of 5 mL PVP-55(20 mg/mL). After another 2 min, 1.6 mL of CF_3COOAg (282 mM) was added into above mixture. Within 15 min, the mixture had reached a brown color, indicating completion of the reaction. The final product was collected by centrifugation and washed repeatedly with acetone and distilled water for characterization and further study.

Preparation of Au-Ag Hollow Nanocube: For a typical synthesis of Au-Ag hollow nanocube, 4 mL of PVP-55 (1 mM) solution was added into a 18 mL glass vial. Then, 1 mL of AA (10 mM), 0.2 mL of HCl (100 mM) and 0.02 mL of Ag nanocubes (4.92 mg/mL) were introduced into above glass vial under magnetic stirring. Following that, 0.8 mL of $HAuCl_4$ solution (0.1 mM) was added dropwise into the solution at a rate of 0.02 mL/min and stired for 10 min. Finally, the product was washed with water thoroughly prior to further use.

2.3. Synthesis of DNA_1-N,S-CDs

In a typical procedure of N,S-CDs preparation.[30] Firstly, 2 g of citric acid and 1 g of L-cysteine were dissolved in 2 mL of distilled water. Then, the solution was heated at 70 ºC for 24 h to form thick syrup. Subsequently, The resultant thick syrup mixture was transferred into a Teflon-lined autoclave and heated at 200 ºC for 2 h with a heating rate of 10 ºC/min. After neutralized to pH 7.0 with NaOH, the supernatant was collected by dialyzing against distilled water. The as-prepared N,S-CDs were stored at 4 ºC for further use. Following that, the N,S-CDs was dispersed in 3 mL of 2.5% glutaraldehyde solution. The mixture was stirred for 2 h. Then, 200 μL of DNA_1 (10 μM) was introduced into above solution to react for 45 min at room temperature. The DNA_1-N,S-CDs was obtained.

2.4. Synthesis of Probe

$ZnFe_2O_4$ nanoparticles were prepared according to the reference.[31] Briefly, 0.34 g of $ZnCl_2$ and 1.35 g of $FeCl_3 \cdot 6H_2O$ were dissolved in 40 mL ethylene glycol with vigorous sonication 30 min. Then 3.6 g of NaAc and 1.0 g of polyethylene glycol-4000 were added into the solution, and the mixture was incubated for 30 min with vigorous shaking, yielding a stable bottle-yellow homogeneous emulsion. After that, the resulting mixture was transferred to a 50 mL Teflon-lined stainless autoclave. The reaction was allowed to proceed for 8 h at 200 ºC. Finally, the black products were rinsed with ethanol and dried in a vacuum oven.

$ZnFe_2O_4$@Au-Ag hollow nanocube were synthesized via a layer-by-layer assembly approach. 20.0 mg of $ZnFe_2O_4$ nanopartcles was dispersed using 2 mL of water. 1 mL 1% PDDA solution was added into the solution, and the mixture was

sonicated for 30 min. The final products were washed several times with water. Following that, 1 mL of the Au-Ag hollow nanocube was introduced into $ZnFe_2O_4$/PDDA nanocomposites under stirring for 1h. The final product was separated by applying an external magnetic field and then redispersed in water.

To obtain the probe, DNA_1-N,S-CDs were modified on the surface of $ZnFe_2O_4$@Au-Ag according to the previous report[32,33] and a detailed procedure was described in the supporting information.

2.5. Preparation of Cy3-17DS-CeO_2

In a typical synthesis,[34] 0.374 g $Ce(NO_3)_3 \cdot 6H_2O$, 0.09 g HMT and 0.4 g PVP were dissolved in 16 mL distilled water. After that, the mixture was transferred into a Teflon-lined autoclave and maintained at 180 ºC for 100 min, then cooled to room temperature. The precipitates were separated by centrifuging and washed with distilled water several times.

Preparation of Cy3-17DS-CeO_2: Firstly, the CeO_2 surface was silylated with APTES. Then, amino-functionalized CeO_2 were dispersed in a mixture of 200 μL Cy3-17DS (10 μM), 100 μL EDC (20 mg mL^{-1}) and 50 μL NHS (20 mg mL^{-1}). And the mixture was stirred for 12 h. The Cy3-17DS-CeO_2 was collected by centrifugation and extensively washed with water.

2.6. Operation and assay procedures of this biosensor

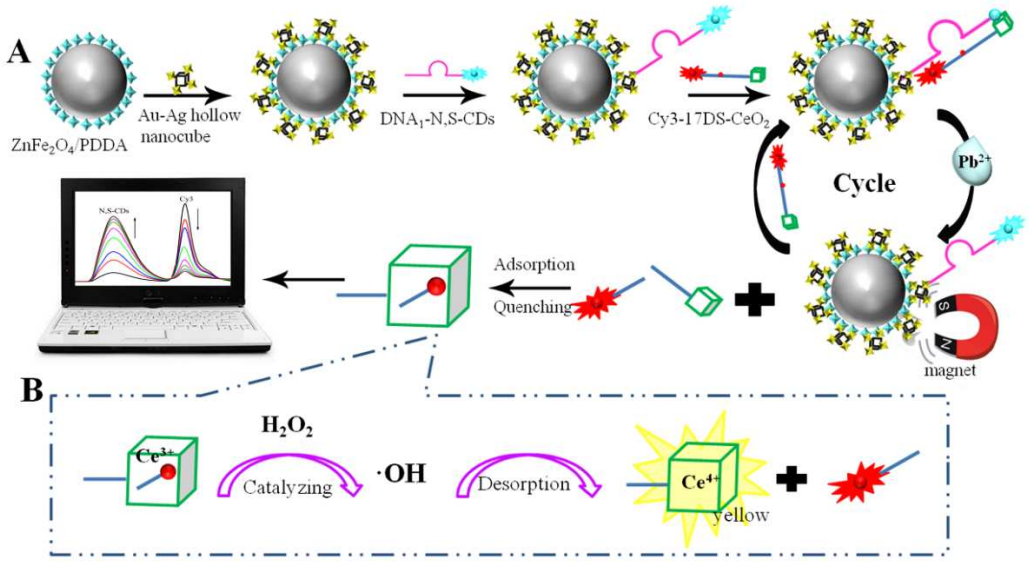

Scheme 1. Schematic illustration of the stepwise Pb^{2+} biosensor fabrication process.

The fabrication and the assay procedure for preparing the Pb^{2+} biosensor are represented in Scheme 1. Firstly, the probe was incubated with excess Cy3-17DS-CeO_2 for 16 h at 37 ºC to form a dsDNA structure. And then the mixture was magnetically washed with PBS to remove surplus Cy3-17DS-CeO_2. Next, various concentrations of Pb^{2+} were allowed to react with the above solution for 60 min at 37 ºC to obtain maximum cleavage of the substrate strands. Firstly, Preliminary test of Pb^{2+} was performed by naked eye. After magnetic separation, 2% H_2O_2 was introduced into supernatant. A fast color change occurred, which could be easily judged by the naked eye. If necessary, precise ratiometric fluorescence detection was implemented, the ratio of the fluorescence intensity at 562 and 424 nm was acted as an ideal ratiometric sensor for quantitative analysis of Pb^{2+}. Finally, upon supplementation of Cy3-17DS-CeO_2 in precipitate, the dsDNA structure is regenerated by means of rehybridization between Cy3-17DS-CeO_2 and probe, leading to fabricate a recyclable Pb^{2+} biosensor.

3. Results and discussion

3.1. Characterization of Bifunctional Nanocomposite $ZnFe_2O_4$, Au-Ag and $ZnFe_2O_4$@Au-Ag

The bifunctional nanocomposite was prepared via a layer-by-layer assembly process, which involved Au-Ag hollow nanocube synthesis, $ZnFe_2O_4$ synthesis, and final assembly of Au-Ag hollow nanocube onto the $ZnFe_2O_4$ surfaces. As a general and

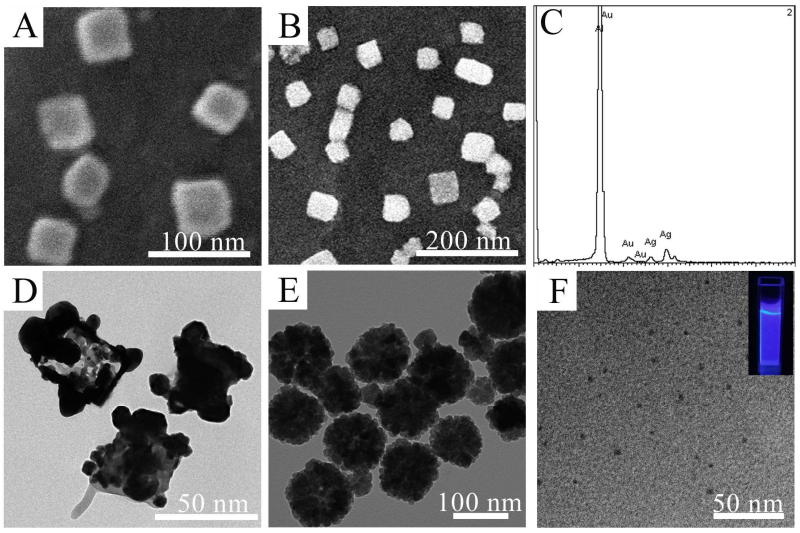

Fig. 1. SEM images of (A) Ag nanocubes; (B) Au-Ag hollow nanocube. (C) EDX images of Au-Ag hollow nanocube. TEM images of (D) Au-Ag hollow nanocube; (E) $ZnFe_2O_4$. (F) TEM images of N,S-CDs. Inset: photograph of N,S-CDs under UV light.

effective method for synthesizing metallic nanostructures, galvanic replacement reaction has been used. We have paid close attention to Ag nanocubes because it possesses well-defined facets and monodispersed size. The morphology of the prepared Ag nanocubes was shown in Fig. 1A. Scanning electron microscopy (SEM) image was clearly found that the average edge length of Ag nanocubes was 49.0 nm, together with slightly rounded corners. Since the standard reduction potential of the Ag^+/Ag (0.80 V

vs standard hydrogen electrode, SHE) is lower than that of the $AuCl_4^-$/Au (0.99 V vs SHE), the loaded Ag nanocrystals would be oxidized into Ag^+ with the addition of $HAuCl_4$ in an aqueous medium. The reaction equation is described as follows.

$$3Ag(s)+AuCl_4^-(aq)=Au(s)+3Ag^+(aq)+4Cl^-(aq)$$

More importantly, pH plays an essential role in controlling morphology and ultimately achieving galvanic replacement free deposition of Au on Ag nanocubes. When the pH was adjusted to 2.63 with the addition of HCl and $HAuCl_4$, we observed the formation of Ag-Au hollow nanocubes. The morphologies of Ag-Au hollow nanocubes were characterized by SEM and transmission electron microscopy (TEM). As shown in Fig. 1B, the hollow nanostructures essentially retained their original cubic shape. The energy dispersive X-ray spectroscopy (EDS) analyses (Fig. 1C) of Ag-Au hollow nanocubes showed that the sample consisted of Au and Ag elements. And the TEM (Fig. 1D) showed hollow nanoparticles with multiple pores in the walls. These indicated that the galvanic reaction took a leading in an acidic solution, which was consistent with the previous findings. Furthermore, a surface-enhanced raman scattering activity of the Ag-Au hollow nanocubes were stronger than that of the Ag nanocubes (Fig. 2A). As for one of the key constituent of this bifunctional nanocomposite, $ZnFe_2O_4$ were synthesized according to the earlier report and characterized by TEM. Fig. 1E showed well-defined spinel ferrite compounds, which were spherical and dispersive with an average size of about 100 nm. The result was consistent with the X-ray diffraction (XRD) data analysis (Fig. 2B). In addition, FT-IR was used to identify the functional groups of the $ZnFe_2O_4$ (Fig. S1).

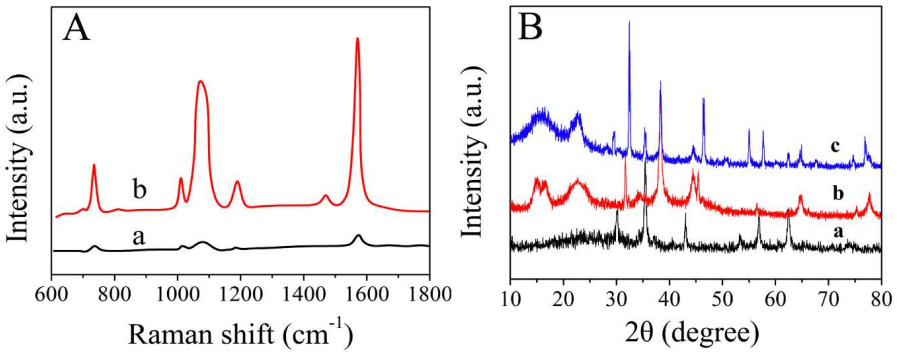

Fig. 2. (A) Comparison of raman spectra of the Ag nanocubes (a), Ag-Au hollow nanocubes (b). (B) XRD patterns of the as-prepared Au-Ag hollow nanocubes (a), $ZnFe_2O_4$ (b) and $ZnFe_2O_4$@Au-Ag (c)

To further characterize the successful preparation of $ZnFe_2O_4$@Au-Ag, the XRD patterns and evolution of ζ-potentials were performed. XRD of the as-prepared Au-Ag hollow nanocube, $ZnFe_2O_4$ and $ZnFe_2O_4$@Au-Ag were shown in Fig. 2. In curve a, five diffraction peaks appeared at 31.9, 39.4, 45.8, 66.2 and 78.8º, which were coincidently located between Au (reference code: 00-004-0784) and Ag (reference code: 00-005-0681), indicating the successful fabrication of Au-Ag hollow nanocube. In curve b, the diffraction peaks at 30.0, 35.4, 43.0, 53.2, 56.8 and 62.5º could be indexed to (220), (311), (400), (422), (511) and (440) crystal planes of $ZnFe_2O_4$ spinel structure, respectively. All the diffraction peaks could be matched well with the $ZnFe_2O_4$ standard spinel-type patterns (JCPDS 22-1012). However, in curve c, it could be seen that the typical peaks of $ZnFe_2O_4$ were weak/disappeared and the diffraction peaks of Au-Ag hollow nanocube were observable. These results demonstrated that the $ZnFe_2O_4$ were successfully decorated with Au-Ag hollow nanocube, which were consistent with the

corresponding ζ-potentials spectra (Fig. S2).

3.2.Characterization of N,S-CDs and CeO_2

The TEM images (Fig. 1F) indicated that the used N,S-CDs were uniform and well dispersed with an average diameter of 5.1 nm. The remarkable optical properties of the N,S-CDs were investigated by the UV-vis absorption and fluorescence spectra. For the UV-vis absorption (Fig. 3A), the N,S-CDs showed a sharp peak centered around 362 nm. The fluorescence spectra exhibited the emission wavelength of the N,S-CDs was nearly excitation-independent (Fig. 3A), with the maximum excitation wavelength and the maximum emission wavelength at 360 and 424 nm, respectively.

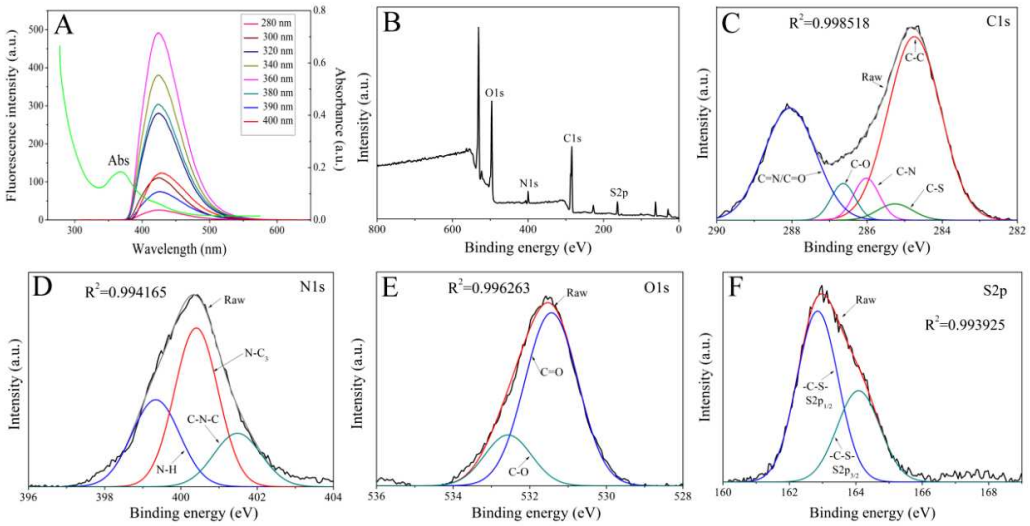

Fig. 3. (A) UV and fluorescence spectra of the N,S-CDs. The fluorescence spectra were recorded from 280 to 400 nm. (B) XPS spectra of the obtained N,S-CDs. (C-F) High-resolution XPS spectra of the C1s, N1s, O1s and S2p of the N,S-CDs, respectively.

The N,S-CDs displayed narrow and symmetrical fluorescence spectra, resulting from their narrower size distribution. In addition, the N,S-CDs exhibited strong blue luminescence under excitation at 365 nm (inset in Fig. 1F), and its QY was up to

54.4%.[35] Such a strong fluorescence was ascribed to the nitrogen sulfur doping undoubtedly.

The XPS was employed to investigate the surface composition and elemental analysis of N,S-CDs (Fig. 3). The full range XPS analysis of N,S-CDs (Fig. 3B) clearly showed four typical peaks of C1s (284 eV), N1s (406 eV), O1s (496 eV) and S2p (185 eV).[36] The higher resolution spectrum of C1s (Fig. 3C) could be deconvoluted into five peaks at C-C/C=C (284.7 eV), C-S (285.3 eV), C-N (286.0 eV), C-O (286.6 eV), C=O/C=N (288.0 eV).[37] The N1s spectrum (Fig. 3D) displayed three peaks at 399.3, 400.4 and 401.5 eV, which represented N1s states in C-N-C, C_2-N-H and N-C_3 bonds,[38] respectively. The two fitted peaks at 531.4 and 532.6 eV in O1s spectrum (Fig. 3E) belonged to C=O and C-O groups, respectively.[39] The S2p spectrum (Fig. 3F) could be resolved into two peaks at 163.5 and 164.6 eV, owing to the $2p_{3/2}$ and $2p_{1/2}$ of the -C-S- covalent bond, respectively.[40] The surface components of the N,S-CDs determined by the XPS were consistent with the corresponding FT-IR spectra (Fig. S3).

The morphologies of the CeO_2 were observed by SEM and TEM. SEM observation of the CeO_2 (Fig. 4A) suggested that the products had a good dispersibility and a narrow distribution of diameters in the range of 13-15 nm. Similar results were obtained by the corresponding TEM characterization (Fig. 4B). XRD

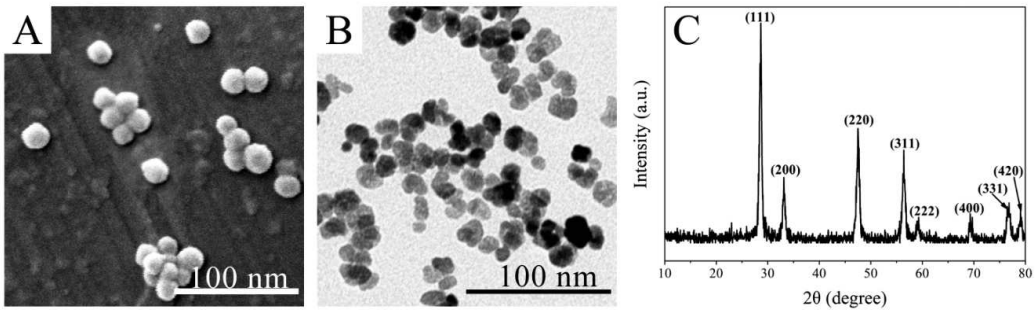

Fig. 4. (A) SEM image, (B) TEM images, and (C) XRD pattern of the typical CeO_2 nanoparticles.

patterns of the as-prepared CeO_2 were shown in Fig. 4C. The peaks at 2θ values of 28.6, 33.1, 47.5, 56.4, 59.3, 69.3, 76.8 and 79.0 could be indexed to (111), (200), (220), (311), (222), (400), (331) and (420) crystal planes, respectively. All the diffraction peaks could be directly indexed to a pure phase of face-centered cubic ceria structures (JCPDS 34-0394), which were consistent with the corresponding TEM or SEM.

3.3. Possible mechanism for the proposed biosensor

The bifunctional nanocomposite was used for building Pb^{2+} biosensor by conjugation with double-stranded DNA, which included Pb^{2+}-specific DNAzyme strand (DNA_1-N,S-CDs) and corresponding substrate strand (Cy3-17DS-CeO_2). The mechanism of metal-enhanced ratiometric fluorescence biosensor was shown in Scheme 1A. In the absence of Pb^{2+}, the formation of double-stranded DNA bringed the labeled N,S-CDs and superquencher CeO_2 into close proximity, which significantly quenching the fluorescence of N,S-CDs. Moreover, and the intensity of Cy3 could be enhanced by the MEF effect (Fig. S4). Upon the addition of Pb^{2+}, the DNAzyme strand was activated and cleaved the substrate strand at the cleavage site (red dot) into two parts, releasing free DNAzyme strand and two fragments.[41,42] The N,S-CDs labeled at one end of DNAzyme strand stayed away from the CeO_2, generating strong fluorescence signals. This moment, N,S-CDs was close to the Ag-Au hollow nanocubes to enhance its fluorescence, and thus the sensitivity of biosensor was obviously improved. And due to CeO_2 not only strongly quenches fluorescence but also adsorbs DNA, indicating very high fluorescence quenching efficiency for Cy3 by CeO_2.

As illustrated in Scheme 1B, it is generally accepted that after adding H_2O_2, Ce^{3+} is quickly oxidized Ce^{4+}, yielding the color change and DNA desorption.[43-45] The reaction equation is described as follows:

$$Ce^{3+} + H_2O_2 + H^+ \rightarrow Ce^{4+}\text{ (yellow)} + \cdot OH + H_2O$$

3.4. Metal-enhanced ratiometric fluorescence and naked eye detection of Pb^{2+}

The feasibility of the proposed biosensor was investigated in the detection of Pb^{2+}. Under the optimal experimental conditions (Fig. S5), firstly, preliminary test of Pb^{2+} was executed by naked eye. After magnetic separation, 2% H_2O_2 was introduced into supernatant. The color changes could be readily observed by the naked eye. The results were shown in Fig. 5A, the color turned from colorless to yellow to a deep with increasing concentrations of Pb^{2+} (inset). Moreover, the proposed biosensor showed a good linear relationship between the absorbance and the concentrations of Pb^{2+}, which indicated the particularly attractive for visually sensing of Pb^{2+}. In addition, if necessary, precise ratiometric fluorescence detection induced by different concentrations of Pb^{2+} was evaluated. As shown in Fig. 5B, with the Pb^{2+} concentration increasing, the fluorescence intensity of Cy3 (I_{562}) decreased, and the

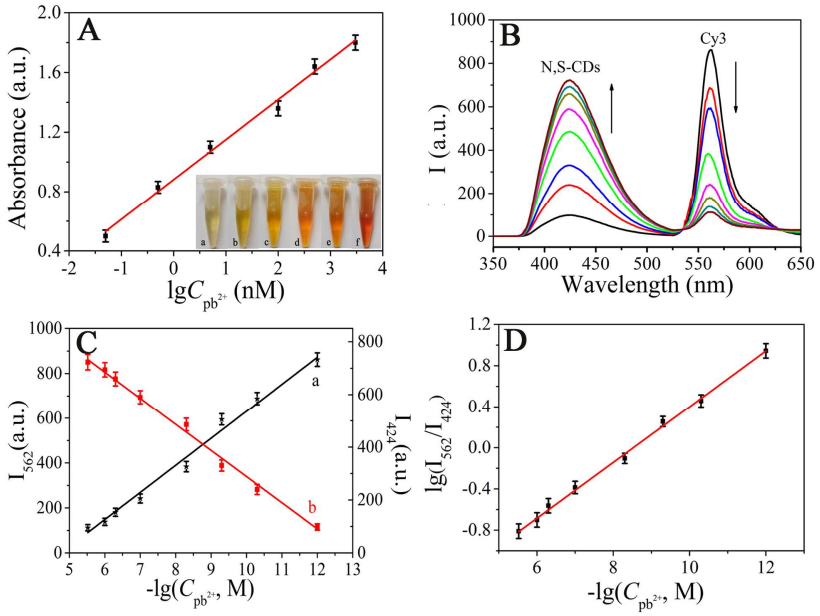

Fig. 5. (A) Naked eye response of Pb^{2+} at the concentrations of 0.05, 5, 100, 500, 1000, 3000 nM (a-f). Inset: photo of the above samples. (B) Ratio fluorescence responses of this biosensor towards different concentrations of Pb^{2+} from 0.001 to 3000 nM in pH 7.4 PBS buffer. (C) Relationship between the I_{562} (a) and I_{424} (b) to the concentration of the Pb^{2+}. (D) Relationship between the lg(I_{562}/I_{424}) and the concentration of Pb^{2+}.

fluorescence intensity of N,S-CDs (I_{424}) increased correspondingly. Fig. 5C showed the relationship between Pb^{2+} concentration and fluorescence intensity toward I_{562} (a) and I_{424} (b). The regression equations were I_{562} = 120.6lg$c$ – 575.0 with the R^2 of 0.990 and I_{424} = -99.05lg$c$ + 1279 with the R^2 of 0.995. To improve fluorescence accuracy, we utilized the ratiometric method to detect the Pb^{2+} by calculating the ratio of I_{562} and I_{424}. In accordance with Fig. 5D, the corresponding regression equation could be represented as lg(I_{562}/I_{424}) = -0.2713lg$c$ – 2.312 (correlation coefficient, R^2 = 0.995), where c represent the concentration of Pb^{2+}. The detection limit for Pb^{2+} was calculated to be 3×10^{-13} M (3σ), with a linear range of 10^{-12}-3×10^{-6} M, proving the potential of the proposed biosensor for sensitive detection of Pb^{2+}. Compared with other methods

reported previously, our proposed pb^{2+} biosensor exhibited a better performance, especially the detection limit (the details can be found in the Table S1).

3.5. Recyclability, stability, reproducibility and specificity of the biosensor

It was worth mentioning that most of current Pb^{2+} biosensor could not be cyclically used.[46,47] Hence, it was strongly hope to structure a recyclable Pb^{2+} biosensor. As described in Fig. 6A, Cy3-17DS-CeO_2 was cleaved into two free DNA fragments in the presence of Pb^{2+}. After the first round reaction with Pb^{2+}, which was magnetic washed with 0.1 M PBS buffer solution (pH 7.4) for several times to remove the free

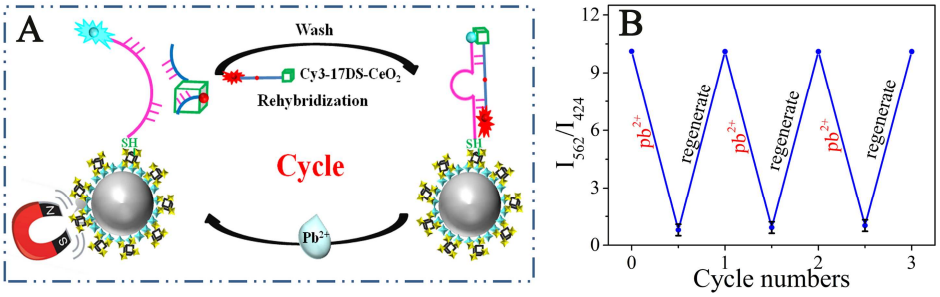

Fig. 6. (A) Schematic illustration of regeneration of signal probe through the supplementation of Cy3-17DS-CeO_2. (B) corresponding I_{562}/I_{424} when the signal probe is recycling for three times in the detection of 5 nM Pb^{2+}.

DNA fragments and Pb^{2+}. Upon supplementation of Cy3-17DS-CeO_2, the dsDNA structure was regenerated by the rehybridization between Cy3-17DS-CeO_2 and DNA_1-N,S-CDs. Hence, the recyclability of such biosensor for the detection of Pb^{2+} was evaluated through the consecutive reaction cycles. The detection results were revealed in Fig. 6B. It displayed that the Pb^{2+} biosensor could be repeated at least three times without significant change of the fluorescence intensity, declaring the good recyclability of such Pb^{2+} biosensor.

An essential factor of the proposed biosensor in their application and development is the stability. In order to verify the stability of the proposed biosensor, it was stored at 4 ºC in the refrigerator. As revealed in Fig. 7A, compared with the initial response, the I_{562}/I_{424} intensity of the proposed biosensor has changed little after 5 weeks. These results demonstrated that the proposed biosensor exhibited remarkable stability and was fairly robust in normal storage conditions.

The reproducibility of the proposed biosensor was also crucial requirements for any practical applications, which was evaluated by intra- and inter-assay relative standard deviation (RSD). The proposed biosensor prepared on the same and different batches were used to detect 5 nM Pb^{2+}, respectively. These results indicated that their RSDs of five parallel determinations were 3.8% for the same batch biosensor, and 4.6% for different batch biosensor, demonstrating an acceptable reproducibility and precision of the proposed method.

To examine the specificity of the proposed biosensor toward Pb^{2+}, experiments were performed by parallelly using 7 kinds of other competing metal ions (e.g., Fe^{3+}, Hg^{2+}, Zn^{2+}, Ag^{+}, Cu^{2+}, Na^{+}, Cd^{2+}), the mixture samples including all metal ions (mix) and 4 kinds of natural organic matters. As shown in Fig. 7B, it showed that the I_{562}/I_{424} signal of above possible interference ions and natural organic matters were almost the same as the background response intensity. In addition, the mixture samples did not obviously reveal I_{562}/I_{424} change compared with that of Pb^{2+} alone. As a consequence, this comparison essentially demonstrated that the proposed biosensor had an excellent selectivity, declaring its potential application in complex samples analysis.

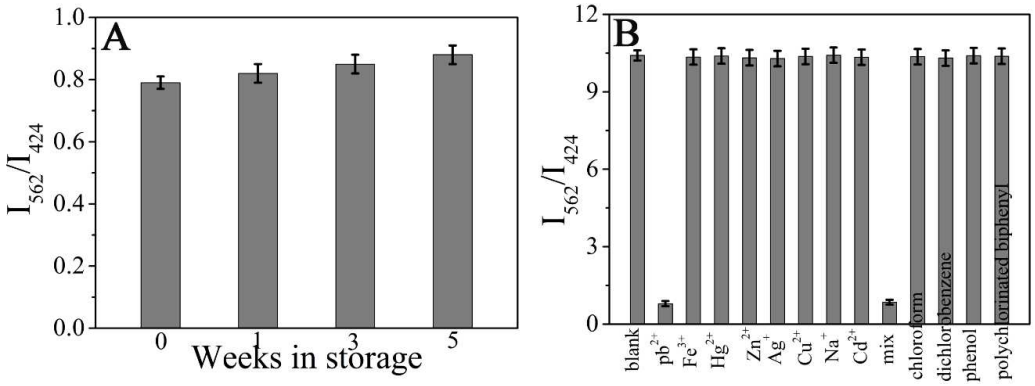

Fig. 7. (A) the stability of the Pb^{2+} biosensor; and (B) specificity of the Pb^{2+} biosensor over several metal ions and natural organic matters (the concentration of Pb^{2+} was 5 nM).

3.6. Application of the biosensor in lake water

The proposed biosensor not only possessed predominant selectivity, acceptable reproducibility, ultrahigh sensitivity but also excellent recyclability. This character may apply a promising candidate for identification of Pb^{2+} in real samples. Subsequently, 50 μL of freshwater spiked with different concentrations of Pb^{2+} was dropped onto the proposed biosensor. The results were shown in Table 1, the recovery values ranged from 95.80-104.0%. This result agrees well with the ICP-MS result, demonstrating that the accuracy our method is as good as that of the standard ICP-MS

Table 1 The determination of unknown Pb^{2+} in lake water samples.

Sample	Add/nM	Found/nM	Recovery/%	ICP-MS
Lake Water	0.5	0.52	104.0	0.51
	10.0	9.58	95.80	9.89
	100.0	99.47	99.47	99.54
	1000.0	9831.0	98.31	9901.0

method for real sample analysis. Therefore, the proposed biosensor was acceptable for real applications of Pb^{2+} from lake water with other potentially competitive species coexistence.

4. Conclusions

In summary, we have successfully developed a ultrasensitive, recyclable, selective and ratiometric determination of trace Pb^{2+} based on $ZnFe_2O_4$@Au-Ag bifunctional nanocomposite and DNA/CeO_2 complex. The detection idea of the proposed biosensor included preliminary visual inspection by color change and accurate ratiometric fluorescence detection. The detection results could be also visually observed with high specificity. Aside from Au-Ag hollow nanocube enhanced fluorescence intensity by MEF effect and improved the sensitivity of the proposed biosensor, the resultant biosensor featured a good specificity and remarkable sensitivity. Besides, the proposed biosensor also possessed good capability of recycling in three cycles by means of the supplementation of Cy3-17DS-CeO_2. More significantly, the developed biosensor was further certified to be applicable in the detection of Pb^{2+} from real samples with high recoveries.

Associated content

Supporting Information

FT-IR spectra for $ZnFe_2O_4$, evolution of ζ-potentials during the layer-by-layer assembly processes, FT-IR spectra for N,S-CDs, verify the superiority of the Au-Ag hollow nanocube-based MEF biosensor, optimization of metal-enhanced FRET

biosensor, stability in different ionic strength environments, assay results of Pb^{2+} using the proposed and referenced biosensors. This material is available free of charge via the Internet at http://pubs.acs.org.

Author information

Corresponding Author

*E-mail: chm_gesg@163.com. Phone: +86-531-82767161.

Notes

The authors declare no competing financial interest.

Acknowledgements

This work was financially supported by National Natural Science Foundation of China (21575051, 21475052, 51502112), National High-tech R & D Program (863 Program, 2015AA034701), and Key Research and Development Program of Shandong Province, China (2016GGX102035).

References

(1) Hong, G. S.; Tabakman, S. M.; Welsher, K.; Wang, H. L.; Wang, X. R.; Dai, H. J. *J. Am. Chem. Soc.* **2010**, 9, 15921-15923.

(2) Aslan, K.; Gryczynski, I.; Malicka, J.; Matveeva, E.; Lakowicz, J. R.; Geddes, C. D. *Curr. Opin. Biotechnol.* **2005**, 16, 55-62.

(3) Zhang, J.; Fu, Y.; Chowdhury, M. H.; Lakowicz, J. R. *J. Phys. Chem. C* **2008**, 112, 18-26.

(4) Wang, Y.; Li, Z.; Li, H.; Vuki, M.; Xu, D.; Chen, H. Y. *Biosens. Bioelectron.* **2012**, 32, 76-81.

(5) Yang, Y.; Liu, J. Y.; Fu, Z. W.; Qin, D. *J. Am. Chem. Soc.* **2014**, 136, 8153-8156.

(6) Su, L.; Feng, J.; Zhou, X. M.; Ren, C. L.; Li, H. H.; Chen, X. G. *Anal. Chem.* **2012**, 84, 5753-5758.

(7) Rusling, J. F.; Sotzing, G.; Papadimitrakopoulosa, F. *Bioelectrochemistry* **2009**, 76, 189-194.

(8) Nash, M. A.; Waitumbi, J. N.; Hoffman, A. S.; Yager, P.; Stayton, P. S. *ACS Nano* **2012**, 6, 6776-6785.

(9) Laberty-Robert, C.; Long, J. W.; Pettigrew, K. A.; Stroud, R. M.; Rolison, D. R. *Adv. Mater.* **2007**, 19, 1734-1739.

(10) Ornatska, M.; Sharpe, E.; Andreescu, D.; Andreescu, S. *Anal. Chem.* **2011**, 83, 4273-4280.

(11) Xu, C.; Liu, Z.; Wu, L.; Ren, J.; Qu, X. *Adv. Funct. Mater.* **2014**, 24, 1624-1630.

(12) Pautler, R.; Kelly, E. Y.; Huang, P.-J. J.; Cao, J.; Liu, B.; Liu, J. *ACS Appl. Mater.*

Interfaces **2013**, 5, 6820-6825.

(13) He, Q. W.; Miller, E. W.; Wong, A. P.; Chang, C. J. *J. Am. Chem. Soc.* **2006**, 128, 9316-9317.

(14) Lu, Y.; Li, X.; Wang, G. K.; Tang, W. *Biosens. Bioelectron.* **2013**, 39, 231-235.

(15) Dalavoy, T. S.; Wernette, D. P.; Gong, M.; Sweedler, J. V.; Lu, Y.; Flachsbart, B. R.; Shannon, M. A.; Bohn, P. W.; Cropek, D. M. *Lab Chip* **2008**, 8, 786-793.

(16) Xiao, Y.; Rowe, A. A.; Plaxco, K. W. *J. Am. Chem. Soc.* **2007**, 129, 262-263.

(17) Pelossof, G.; Tel-Vered, R.; Willner, I. *Anal. Chem.* **2012**, 84, 3703-3709.

(18) Liu, J.; Lu, Y. J. *J. Am. Chem. Soc.* **2005**, 127, 12677-12683.

(19) Wang, Z.; Lee, J. H.; Lu, L. *Adv. Mater.* **2008**, 20, 3263-3267.

(20) Wang, H.; Kim, Y.; Liu, H.; Zhu, Z.; Bamrungsap, S.; Tan, W. *J. Am. Chem. Soc.* **2009**, 131, 8221-8226.

(21) Zhao, X. H.; Kong, R. M.; Zhang, X. B.; Meng, H. M.; Liu, W. N.; Tan, W.; Shen, G. L.; Yu, R. Q. *Anal. Chem.* **2011**, 83, 5062-5066.

(22) Wen, Y.; Peng, C.; Li, D.; Zhuo, L.; He, S.; Wang, L.; Huang, Q.; Xu, Q. H.; Fan, C. *Chem. Commun.* **2011**, 47, 6278-6280.

(23) Xia, J.; Lin, M.; Zuo, X.; Su, S.; Wang, L.; Huang, W.; Fan, C.; Huang, Q. *Anal. Chem.* **2014**, 86, 7084-7087.

(24) Park, M.; Ha, H. D.; Kim, Y. T.; Jung, J. H.; Kim, S. H.; Kim, D. H.; Seo, T. S. *Anal. Chem.* **2015**, 87, 10969-10975.

(25) Liu, Z. G.; Sun, Y. F.; Chen, W. K.; Kong, Y.; Jin, Z.; Chen, X.; Zheng, X.; Liu, J. H.; Huang, X. J.; Yu, S. H. *Small* **2015**, 11, 2493-2498.

(26) Tsien, R. Y.; Poenie, M. *Trends Biochem. Sci.* **1986**, 11, 450-455.

(27) Srikun, D.; Miller, S. E.; Domaille, D. W.; Chang, C. J. *J. Am. Chem. Soc.* **2008**, 130, 4596-4597.

(28) Kubo, Y.; Yamamoto, M.; Ikeda, M.; Takeuchi, M.; Shinkai, S.; Yamaguchi, S.; Tamao, K. *Angew. Chem. Int. Ed.* **2003**, 42, 2036-2040.

(29) Yang, Y.; Liu, J. Y.; Fu, Z. W.; Qin, D. *J. Am. Chem. Soc.* **2014**, 136, 8153-8156.

(30) Dong, Y. Q.; Cai, J. H.; Fang, Q. Q.; You, X.; Chi. Y. W. *Anal. Chem.* **2016**, 88, 1748-1752.

(31) Deng, H.; Li, X. L.; Peng, Q.; Wang, X.; Chen, J. P.; Li, Y. D. *Angew. Chem. Int. Ed.* **2005**, 117, 2842-2845.

(32) Zhang, X.; Servos, M. R.; Liu, J. W. *J. Am. Chem. Soc.* **2012**, 134, 7266-7269.

(33) Zhang, X.; Servos, M. R.; Liu, J. W. *Chem. Commun.* **2012**, 48, 10114-10116.

(34) Xie, A. R.; Wang, S. P.; Liu, W.; Zhang, J. C.; Yang, Y. Z.; Han, J. T. *Materials Research Bulletin* **2015**, 62, 148-152.

(35) Ding, H.; Wei, J. S.; Xiong, H. M. *Nanoscale* **2014**, 6, 13817-13823.

(36) Dong, Y.; Pang, H.; Yang, H. B.; Guo, C.; Shao, J.; Chi, Y.; Li, C. M.; Yu, T. *Angew. Chem. Int. Ed.* **2013**, 52, 7800-7804.

(37) Liu, S.; Tian, J.; Wang, L.; Zhang, Y.; Qin, X.; Luo, Y.; Asiri, A. M.; Al-Youbi, A. O.; Sun, X. *Adv. Mater.* **2012**, 24, 2037-2041.

(38) Qian, Z.; Ma, J.; Shan, X.; Feng, H.; Shao, L.; Chen, J. *Chem.-Eur. J.* **2014**, 20, 2254-2263.

(39) Lu, W.; Qin, X.; Liu, S.; Chang, G.; Zhang, Y.; Luo, Y.; Asiri, A. M.; Al-Youbi, A.

O.; Sun, X. *Anal. Chem.* **2012**, 84, 5351-5357.

(40) Sun, D.; Ban, R.; Zhang, P. H.; Wu, G. H.; Zhang, J. R.; Zhu, J. J. *Carbon* **2013**, 64, 424-434.

(41) Xiao, Y.; Rowe, A. A.; Plaxco, K. W. *J. Am. Chem. Soc.* **2007**, 129, 262-263.

(42) Shen, L.; Chen, Z.; Li, Y.; He, S.; Xie, S.; Xu, X.; Liang, Z.; Meng, X.; Li, Q.; Zhu, Z.; Li, M.; Le, X. C.; Shao, Y. *Anal. Chem.* **2008**, 80, 6323-6328.

(43) Lee, S. S.; Song, W. S.; Cho, M. J.; Puppala, H. L.; Nguyen, P.; Zhu, H. G.; Segatori, L.; Colvin, V. L. *ACS Nano* **2013**, 7, 9693-9703.

(44) Ornatska, M.; Sharpe, E.; Andreescu, D.; Andreescu, S. *Anal. Chem.* **2011**, 83, 4273-4280.

(45) Sardesai, N. P.; Andreescu, D.; Andreescu, S. *J. Am. Chem. Soc.* **2013**, 135, 16770-16773.

(46) Wang, Y.; Irudayaraj, J. *Chem. Commun.* **2011**, 47, 4394-4396.

(47) Fu, C.; Xu, W.; Wang, H.; Ding, H.; Liang, L.; Cong, M.; Xu, S. *Anal. Chem.* **2014**, 86, 11494-11497.